arXiv:1405.5292v1 [nucl-th] 21 May 2014

Temperature dependence of cross sections for meson-meson nonresonant reactions in hadronic matter

Zhen-Yu Shen and Xiao-Ming Xu

Department of Physics, Shanghai University, Baoshan, Shanghai 200444, China

Abstract

We study unpolarized cross sections for the endothermic nonresonant reactions: $\pi\pi \to \rho\rho$ for $I = 2$, $KK \to K^*K^*$ for $I = 1$, $KK^* \to K^*K^*$ for $I = 1$, $\pi K \to \rho K^*$ for $I = 3/2$, $\pi K^* \to \rho K^*$ for $I = 3/2$, $\rho K \to \rho K^*$ for $I = 3/2$, and $\pi K^* \to \rho K$ for $I = 3/2$, which take place in hadronic matter. We provide a potential that is given by perturbative QCD with loop corrections at short distances, becomes a distance-independent and temperature-dependent value at long distances, and has a spin-spin interaction with relativistic modifications. The Schrödinger equation with the potential yields temperature-dependent meson masses and mesonic quark-antiquark relative-motion wave functions. In the first Born approximation with the quark-interchange mechanism, the temperature dependence of the potential, meson masses and wave functions brings about temperature dependence of unpolarized cross sections for the seven nonresonant reactions. Noticeably, rapid changes of π and K radii cause an increase in peak cross sections while the temperature approaches the critical temperature. Parametrizations of the numerical cross sections are given for their future applications in heavy ion collisions.

PACS: 25.75.-q, 13.75.Lb, 12.38.Mh

Keywords: Cross sections; Quark-interchange mechanism; Meson-meson reactions.

1. Introduction

Heavy ion collisions at the Relativistic Heavy Ion Collider (RHIC) and at the Large Hadron Collider (LHC) produce interesting hadronic matter which final state can be detected. The simplest quantity measured is the ratio of p_T-integrated midrapidity yields for mesons. For central Au+Au collisions at $\sqrt{s_{NN}}$=200 GeV ratios from the PHENIX Collaboration are π^-/π^+ =0.984, K^-/K^+ =0.933, K^+/π^+ =0.171, and K^-/π^- =0.162 [1]. The STAR Collaboration obtained ρ^0/π^-=0.169 for peripheral Au+Au collisions at $\sqrt{s_{NN}}$=200 GeV [2], ρ^0/π^-=0.23 for midcentral Cu+Cu collisions at $\sqrt{s_{NN}}$=200 GeV [3], and K^{*0}/K^-=0.2 for central Au+Au collisions at $\sqrt{s_{NN}}$=200 GeV [4]. For central Pb+Pb collisions at $\sqrt{s_{NN}}$ = 2.76 TeV ratios from the ALICE Collaboration are π^-/π^+=1, K^-/K^+=1, K^+/π^+=0.15, and K^-/π^-=0.15 [5]. The ratios indicate that pions, rhos, and kaons are dominant species in hadronic matter. In the present work we concern ourself about nonresonant reactions among π, ρ, K, and K^* mesons, and focus on cross sections for the endothermic nonresonant reactions: $\pi\pi \to \rho\rho$ for $I = 2$, $KK \to K^*K^*$ for $I = 1$, $KK^* \to K^*K^*$ for $I = 1$, $\pi K \to \rho K^*$ for $I = 3/2$, $\pi K^* \to \rho K^*$ for $I = 3/2$, $\rho K \to \rho K^*$ for $I = 3/2$, and $\pi K^* \to \rho K$ for $I = 3/2$. Cross sections for the inverse reactions of the seven reactions are obtained by the detailed balance.

The mechanism that governs meson-meson nonresonant reactions is the quark-interchange process. With a choice of Gaussian quark-antiquark wave functions the experimental data of S-wave elastic phase shifts for $\pi\pi$ scattering for $I = 2$ and $K\pi$ scattering for $I = 3/2$ in vacuum can be reproduced [6,7]. Good quark-antiquark wave functions are solutions of the Schrödinger equation with a quark potential developed from QCD. Since nonperturbative QCD is not solved, the quark potential is not unique. Meson-meson nonresonant reactions have been studied in different quark potential models. Dissociation cross sections of charmonia in collisions with π and ρ mesons were calculated in Refs. [8,9] with the color Coulomb, spin-spin hyperfine, and linear confining interactions. In a quark model with the potential that arises from one-gluon exchange plus perturbative one- and two-loop corrections at the short distance and exhibits a linear form at the long

distance, we calculated unpolarized cross sections for the seven nonresonant reactions in vacuum [10]. Hadronic matter attracts our attention from the nonresonant reactions in vacuum to those in medium. One effect produced by high-temperature medium is that the linear confinement at the long distance is replaced by a distance-independent value which depends on temperature [11]. In Ref. [10] the spin-spin interaction contains the Fermi contact term and the term that originates from the perturbative one- and two-loop corrections to the one-gluon exchange [12]. The Fermi contact term contains the function $\delta^3(\vec{r})$ which can not be used in the Schrödinger equation. Then, quark-antiquark wave functions are given by the Schrödinger equation with only the central spin-independent potential, and π and ρ mesons (K and K^*) have identical quark-antiquark relative-motion wave functions. In the present work the function $\delta^3(\vec{r})$ in the Fermi contact term is smeared to include relativistic effects as done in Refs. [13, 14] for meson spectra and in Refs. [8, 9] for charmonium dissociation cross sections in vacuum. This smearing significantly changes temperature dependence of π and K masses, and causes different quark-antiquark relative-motion wave functions of π and ρ mesons (K and K^*). Hence, the cross sections for the seven nonresonant reactions are expected to change significantly. Now we have arrived at a potential that is given by perturbative QCD with loop corrections at the short distance, becomes a distance-independent and temperature-dependent potential at the long distance, and has the one-gluon-exchange spin-spin interaction smeared. The potential leads to interesting temperature-dependent cross sections for charmonium dissociation in collisions with pions and rhos in hadronic matter [15]. Therefore, we must calculate the cross sections for the seven nonresonant reactions with the quark potential. This is the subject of the present work.

This paper is organized as follows. In the next section we present the potential of which the short-distance part is given by perturbative QCD and of which the long-distance part is provided by the lattice calculations. Temperature-dependent meson masses and mesonic quark-antiquark relative-motion wave functions are obtained from the Schrödinger equation with the potential. In Sec. 3 cross-section formulae are presented, numerical unpolarized cross sections are displayed and parametrized, and relevant discussions are given.

Finally, we summarize the present work in Sec. 4.

2. Meson masses

The potential includes a central spin-independent potential and the smeared spin-spin interaction. The central spin-independent potential is

$$V_{\rm si}(\vec{r}) = -\frac{\vec{\lambda}_a}{2}\cdot\frac{\vec{\lambda}_b}{2}\frac{3}{4}D\left[1.3-\left(\frac{T}{T_{\rm c}}\right)^4\right]\tanh(Ar)+\frac{\vec{\lambda}_a}{2}\cdot\frac{\vec{\lambda}_b}{2}\frac{6\pi}{25}\frac{v(\lambda r)}{r}\exp(-Er), \quad (1)$$

which shows the feature that the potential at long distances is a distance-independent value which decreases with increasing temperature. At short distances no medium screening sets in, and $V_{\rm si}$ is the potential arising from one-gluon exchange plus perturbative one- and two-loop corrections. The loop corrections are a relativistic modification to the one-gluon-exchange central spin-independent potential (the color Coulomb interaction). In the potential $\vec{r}$ is the relative coordinate of constituents a and b, and λ=$\sqrt{\frac{3b_0}{16\pi^2\alpha'}}$ with the Regge slope α'=1.04 GeV^{-2} and $b_0 = 11-\frac{2}{3}N_f$. In the case of four quark flavors $N_f = 4$, $A = 1.5[0.75+0.25(T/T_{\rm c})^{10}]^6$ GeV, $D = 0.7$ GeV, and $E = 0.6$ GeV. The function $v(x)$ is defined as [16]:

$$v(x) = \frac{4b_0}{\pi}\int_0^\infty \frac{dQ}{Q}(\rho(\vec{Q}^2)-\frac{K}{\vec{Q}^2})\sin(\frac{Q}{\lambda}x),$$

where the quantity $\rho(\vec{Q}^2)-\frac{K}{\vec{Q}^2}$ with $K=\frac{3}{16\pi^2\alpha'}$ is from the one-gluon exchange plus the perturbative one- and two-loop corrections, and Q equals the absolute value of the gluon momentum $\vec{Q}$.

The smeared spin-spin interaction is [15]

$$V_{\rm ss}(\vec{r}) = -\frac{\vec{\lambda}_a}{2}\cdot\frac{\vec{\lambda}_b}{2}\frac{16\pi^2}{25}\frac{d^3}{\pi^{3/2}}\exp(-d^2r^2)\frac{\vec{s}_a\cdot\vec{s}_b}{m_a m_b}+\frac{\vec{\lambda}_a}{2}\cdot\frac{\vec{\lambda}_b}{2}\frac{4\pi}{25}\frac{1}{r}\frac{d^2v(\lambda r)}{dr^2}\frac{\vec{s}_a\cdot\vec{s}_b}{m_a m_b}, \quad (2)$$

where $\vec{s}_a$ ($\vec{s}_b$) and m_a (m_b) are the spin and mass of constituent a (b), respectively, and

$$d^2 = \sigma_0^2[\frac{1}{2}+\frac{1}{2}(\frac{4m_a m_b}{(m_a+m_b)^2})^4]+\sigma_1^2(\frac{2m_a m_b}{m_a+m_b})^2, \quad (3)$$

with $\sigma_0 = 0.15$ GeV and $\sigma_1 = 0.705$.

The first term in the spin-spin interaction is a modification (smearing) of the Fermi contact term $-\frac{\vec{\lambda}_a}{2}\cdot\frac{\vec{\lambda}_b}{2}\frac{16\pi^2}{25}\delta^3(\vec{r})\frac{\vec{s}_a\cdot\vec{s}_b}{m_a m_b}$ that comes from the one-gluon exchange between constituents a and b. The smearing is achieved by the regularization $\delta^3(\vec{r})\to\frac{d^3}{\pi^{3/2}}\exp(-d^2r^2)$.

The use of the Fermi contact term in the Schrödinger equation makes it impossible to solve the equation. However, the smearing overcomes the difficulty and in addition incorporates relativistic effects [8, 9, 13, 14]. The second term originates from the perturbative one- and two-loop corrections to the one-gluon exchange. The loop corrections are a relativistic modification to the one-gluon-exchange spin-spin interaction. The potential $V_{\rm si}(\vec{r}) + V_{\rm ss}(\vec{r})$ is a relativized potential.

The smeared spin-spin interaction given in Eq. (2) plus the central spin-independent potential given in Eq. (1) is used in the Schrödinger equation to yield meson masses and mesonic quark-antiquark relative-motion wave functions that differ from one another. Corresponding to the up and down quark masses $m_u = m_d = 0.32$ GeV and the strange quark mass $m_s = 0.5$ GeV, the mass splittings of π, ρ, K, and K^* involved in the present work are $m_\rho - m_\pi = 0.6294$ GeV and $m_{K^*} - m_K = 0.39865$ GeV at $T = 0$ in comparison with the experimental data of 0.6304 GeV and 0.3963 GeV. Temperature dependence of the π, ρ, K, and K^* masses is shown in Fig. 1 where the temperature covers the temperature region of hadronic matter. While temperature increases, the ρ and K^* masses decrease rapidly, and the π and K masses decrease slowly for $0.6 \leq T/T_{\rm c} < 0.88$ and rapidly for $0.88 \leq T/T_{\rm c} < 1$. The π and ρ mesons (K and K^*) become degenerate in mass at $T \to T_{\rm c}$. The π and ρ masses approach zero while the temperature approaches the critical temperature. This tendency is consistent with the dropping mass scenarios in hadronic matter in Refs. [17, 18]. According to the figure, the meson masses in units of GeV in the region $0.6 \leq T/T_{\rm c} < 1$ are parametrized as

$$\begin{aligned}
m_\pi &= 0.221 \left[1 - \left(\frac{T}{0.99T_{\rm c}}\right)^{6.59}\right]^{0.84}, \\
m_\rho &= 0.73 \left[1 - \left(\frac{T}{0.992T_{\rm c}}\right)^{3.67}\right]^{0.989}, \\
m_K &= 0.46 \left[1 - \left(\frac{T}{1.04T_{\rm c}}\right)^{8.58}\right]^{0.88}, \\
m_{K^*} &= 0.84 \left[1 - \left(\frac{T}{1.05T_{\rm c}}\right)^{4.16}\right]. \qquad (4)
\end{aligned}$$

The parametrization of the π mass should be used to replace that given in Eq. (26) of

Ref. [15], which is valid for $0.6 \leq T/T_{\rm c} < 0.97$.

In coordinate space the quark potential

$$V_{ab}(\vec{r}) = V_{\rm si}(\vec{r}) + V_{\rm ss}(\vec{r}), \tag{5}$$

is used in the Schrödinger equation. But in some cases, for example, in calculations of cross sections, the quark potential in momentum space is convenient. The potential in momentum space is the Fourier transform of $V_{ab}(\vec{r})$:

$$\begin{aligned} V_{ab}(\vec{Q}) &= -\frac{\vec{\lambda}_a}{2}\cdot\frac{\vec{\lambda}_b}{2}\frac{3D}{4}\left[1.3-\left(\frac{T}{T_{\rm c}}\right)^4\right][(2\pi)^3\delta^3(\vec{Q}) - \frac{8\pi}{Q}\int_0^\infty dr\frac{r\sin(Qr)}{\exp(2Ar)+1}] \\ &+\frac{\vec{\lambda}_a}{2}\cdot\frac{\vec{\lambda}_b}{2}64\pi E\int_0^\infty dq\frac{\rho(q^2)-\frac{K}{q^2}}{(E^2+Q^2+q^2)^2-4Q^2q^2} \\ &-\frac{\vec{\lambda}_a}{2}\cdot\frac{\vec{\lambda}_b}{2}\frac{16\pi^2}{25}\exp\left(-\frac{Q^2}{4d^2}\right)\frac{\vec{s}_a\cdot\vec{s}_b}{m_a m_b} \\ &+\frac{\vec{\lambda}_a}{2}\cdot\frac{\vec{\lambda}_b}{2}\frac{16\pi^2\lambda}{25Q}\int_0^\infty dx\frac{d^2v\,(x)}{dx^2}\sin\left(\frac{Q}{\lambda}x\right)\frac{\vec{s}_a\cdot\vec{s}_b}{m_a m_b}. \end{aligned} \tag{6}$$

3. Cross sections, numerical results and discussions

Because of the temperature dependence of the quark potential, the meson masses and mesonic quark-antiquark relative-motion wave functions are temperature-dependent. Now we are ready to use the temperature dependence of the potential, masses and wave functions to obtain temperature dependence of cross sections for the endothermic non-resonant reactions: $\pi\pi \to \rho\rho$ for $I = 2$, $KK \to K^*K^*$ for $I = 1$, $KK^* \to K^*K^*$ for $I = 1$, $\pi K \to \rho K^*$ for $I = 3/2$, $\pi K^* \to \rho K^*$ for $I = 3/2$, $\rho K \to \rho K^*$ for $I = 3/2$, and $\pi K^* \to \rho K$ for $I = 3/2$.

A. Cross-section formulae for meson-meson reactions

When hadron-hadron scattering is studied, the center-of-mass motion of the two hadrons needs to be separated to avoid frame-dependent results. One starts the study from a relativistic Hamiltonian or a nonrelativistic Hamiltonian. It is impossible to separate off the center-of-mass motion of the two scattering hadrons without taking any

approximation in the relativistic Hamiltonian, i.e., one can not change the relativistic Hamiltonian [19] so that some terms contain the center-of-mass coordinate and the other terms do not. We may keep quark wave functions as Dirac spinors and the potential in a relativistic form, and replace the relativistic kinetic energy of each quark by the non-relativistic kinetic energy; the center-of-mass coordinate can then be separated off, and relativistic effects still exist [19]. There is not unique relativistic formalism in treating hadron-hadron scattering. Because nonrelativistic quark models have the advantages: clear exhibition of hadron structures, easy formulation, effective explanation of a good many experimental data, and useful applications in many problems, as shown in Sec. 2, we establish the quark potential that is the one-gluon-exchange central spin-independent potential plus relativistic modifications, and use wave functions that are solutions of the Schrödinger equation with the relativized potential. The relativistic modifications are the perturbative one- and two-loop corrections to the gluon propagator [12, 16] and the smearing in the spin-spin interaction [13]. With the relativized potential the center-of-mass motion is still exactly separated off. The center-of-mass system is thus chosen to conveniently study meson-meson scattering $q_1\bar{q}_1 + q_2\bar{q}_2 \to q_1\bar{q}_2 + q_2\bar{q}_1$, and cross sections depend on the momentum $\vec{P}$ of the initial meson $q_1\bar{q}_1$ and the momentum $\vec{P}'$ of the final meson $q_1\bar{q}_2$. $\vec{P}$ and $\vec{P}'$ are related to the Mandelstam variable $s = (P_{q_1\bar{q}_1} + P_{q_2\bar{q}_2})^2$ by

$$\vec{P}^2(\sqrt{s}) = \frac{1}{4s}\{[s - (m^2_{q_1\bar{q}_1} + m^2_{q_2\bar{q}_2})]^2 - 4m^2_{q_1\bar{q}_1}m^2_{q_2\bar{q}_2}\}, \tag{7}$$

$$\vec{P}'^2(\sqrt{s}) = \frac{1}{4s}\{[s - (m^2_{q_1\bar{q}_2} + m^2_{q_2\bar{q}_1})]^2 - 4m^2_{q_1\bar{q}_2}m^2_{q_2\bar{q}_1}\}, \tag{8}$$

where $m_{q_1\bar{q}_1}$ and $P_{q_1\bar{q}_1} = (E_{q_1\bar{q}_1}, \vec{P}_{q_1\bar{q}_1})$ are the mass and the four-momentum of meson $q_1\bar{q}_1$, respectively. Similar notations are established for mesons $q_2\bar{q}_2$, $q_1\bar{q}_2$ and $q_2\bar{q}_1$.

The cross section for $q_1\bar{q}_1 + q_2\bar{q}_2 \to q_1\bar{q}_2 + q_2\bar{q}_1$ in the center-of-mass system is expressed as

$$\sigma(S, m_S, \sqrt{s}, T) = \frac{1}{32\pi s}\frac{|\vec{P}'(\sqrt{s})|}{|\vec{P}(\sqrt{s})|}\int_0^\pi d\theta |\mathcal{M}_{\rm fi}(s,t)|^2 \sin\theta, \tag{9}$$

where S is the total spin of either the two incoming mesons or the two outgoing mesons, m_S is the magnetic projection quantum number of S, $\mathcal{M}_{\rm fi}$ is the transition amplitude, θ is the angle between $\vec{P}$ and $\vec{P}'$, and the Mandelstam variable $t = (P_{q_1\bar{q}_1} - P_{q_1\bar{q}_2})^2$. The

factor $\frac{1}{32\pi s}\frac{|\vec{P}'|}{|\vec{P}|}$ comes from the phase space element, the four-momentum conservation, and the relative flux of one initial meson with respect to another initial meson. While $\sqrt{s}$ increases from the threshold energy of an endothermic reaction, the factor increases very rapidly and then decreases moderately. The center-of-mass coordinate of mesons $q_1\bar{q}_1$ and $q_2\bar{q}_2$ ($q_1\bar{q}_2$ and $q_2\bar{q}_1$) is not involved in the transition amplitude, and the relative motion of constituents q_1, $\bar{q}_1$, q_2, and $\bar{q}_2$ makes a contribution to the transition amplitude.

Meson-meson scattering process $q_1\bar{q}_1 + q_2\bar{q}_2 \to q_1\bar{q}_2 + q_2\bar{q}_1$ to lowest order includes one quark interchange and one gluon exchange. The scattering has two forms: the prior form in which the gluon exchange takes place prior to the quark interchange and the post form in which the quark interchange is followed by the gluon exhange. The two forms of scattering may lead to different values of the transition amplitude $\mathcal{M}_{\rm fi}$ [20–22]. Hence, we denote the transition amplitude in the prior form by $\mathcal{M}_{\rm fi}^{\rm prior}$ and the one in the post form by $\mathcal{M}_{\rm fi}^{\rm post}$. In momentum space $\mathcal{M}_{\rm fi}^{\rm prior}$ and $\mathcal{M}_{\rm fi}^{\rm post}$ are [10]

$$\mathcal{M}_{\rm fi}^{\rm prior} = 4\sqrt{E_{q_1\bar{q}_1}E_{q_2\bar{q}_2}E_{q_1\bar{q}_2}E_{q_2\bar{q}_1}}\int\frac{d^3p_{q_1\bar{q}_2}}{(2\pi)^3}\frac{d^3p_{q_2\bar{q}_1}}{(2\pi)^3}$$
$$\times\psi^\dagger_{q_1\bar{q}_2}(\vec{p}_{q_1\bar{q}_2})\psi^\dagger_{q_2\bar{q}_1}(\vec{p}_{q_2\bar{q}_1})(V_{q_1\bar{q}_2}+V_{\bar{q}_1q_2}+V_{q_1q_2}+V_{\bar{q}_1\bar{q}_2})\psi_{q_1\bar{q}_1}(\vec{p}_{q_1\bar{q}_1})\psi_{q_2\bar{q}_2}(\vec{p}_{q_2\bar{q}_2}), \quad (10)$$

$$\mathcal{M}_{\rm fi}^{\rm post} = 4\sqrt{E_{q_1\bar{q}_1}E_{q_2\bar{q}_2}E_{q_1\bar{q}_2}E_{q_2\bar{q}_1}}$$
$$\times[\int\frac{d^3p_{q_1\bar{q}_1}}{(2\pi)^3}\frac{d^3p_{q_1\bar{q}_2}}{(2\pi)^3}\psi^\dagger_{q_1\bar{q}_2}(\vec{p}_{q_1\bar{q}_2})\psi^\dagger_{q_2\bar{q}_1}(\vec{p}_{q_2\bar{q}_1})V_{q_1\bar{q}_1}\psi_{q_1\bar{q}_1}(\vec{p}_{q_1\bar{q}_1})\psi_{q_2\bar{q}_2}(\vec{p}_{q_2\bar{q}_2})$$
$$+\int\frac{d^3p_{q_2\bar{q}_2}}{(2\pi)^3}\frac{d^3p_{q_2\bar{q}_1}}{(2\pi)^3}\psi^\dagger_{q_1\bar{q}_2}(\vec{p}_{q_1\bar{q}_2})\psi^\dagger_{q_2\bar{q}_1}(\vec{p}_{q_2\bar{q}_1})V_{\bar{q}_2q_2}\psi_{q_1\bar{q}_1}(\vec{p}_{q_1\bar{q}_1})\psi_{q_2\bar{q}_2}(\vec{p}_{q_2\bar{q}_2})$$
$$+\int\frac{d^3p_{q_1\bar{q}_2}}{(2\pi)^3}\frac{d^3p_{q_2\bar{q}_1}}{(2\pi)^3}\psi^\dagger_{q_1\bar{q}_2}(\vec{p}_{q_1\bar{q}_2})\psi^\dagger_{q_2\bar{q}_1}(\vec{p}_{q_2\bar{q}_1})V_{q_1q_2}\psi_{q_1\bar{q}_1}(\vec{p}_{q_1\bar{q}_1})\psi_{q_2\bar{q}_2}(\vec{p}_{q_2\bar{q}_2})$$
$$+\int\frac{d^3p_{q_1\bar{q}_2}}{(2\pi)^3}\frac{d^3p_{q_2\bar{q}_1}}{(2\pi)^3}\psi^\dagger_{q_1\bar{q}_2}(\vec{p}_{q_1\bar{q}_2})\psi^\dagger_{q_2\bar{q}_1}(\vec{p}_{q_2\bar{q}_1})V_{\bar{q}_1\bar{q}_2}\psi_{q_1\bar{q}_1}(\vec{p}_{q_1\bar{q}_1})\psi_{q_2\bar{q}_2}(\vec{p}_{q_2\bar{q}_2})], \quad (11)$$

where $\psi_{ab}(\vec{p}_{ab})$ is the product of color, spin, flavor and relative-motion wave functions of constituents a and b, and satisfies $\int\frac{d^3p_{ab}}{(2\pi)^3}\psi^+_{ab}(\vec{p}_{ab})\psi_{ab}(\vec{p}_{ab}) = 1$, where $\vec{p}_{ab}$ is the relative momentum of a and b.

Cross sections corresponding to the scattering in the prior form and in the post form are

$$\sigma^{\rm prior}(S, m_S, \sqrt{s}, T) = \frac{1}{32\pi s}\frac{|\vec{P}'(\sqrt{s})|}{|\vec{P}(\sqrt{s})|}\int_0^\pi d\theta|\mathcal{M}_{\rm fi}^{\rm prior}(s,t)|^2\sin\theta, \quad (12)$$

and

$$\sigma^{\rm post}(S, m_S, \sqrt{s}, T) = \frac{1}{32\pi s}\frac{|\vec{P}'(\sqrt{s})|}{|\vec{P}(\sqrt{s})|}\int_0^\pi d\theta |\mathcal{M}_{\rm fi}^{\rm post}(s,t)|^2 \sin\theta, \tag{13}$$

respectively. The unpolarized cross section for $q_1\bar{q}_1 + q_2\bar{q}_2 \to q_1\bar{q}_2 + q_2\bar{q}_1$ is

$$\begin{aligned}\sigma^{\rm unpol}(\sqrt{s}, T) &= \frac{1}{(2S_{q_1\bar{q}_1}+1)(2S_{q_2\bar{q}_2}+1)}\sum_S (2S+1) \\ &\times \frac{\sigma^{\rm prior}(S, m_S, \sqrt{s}, T) + \sigma^{\rm post}(S, m_S, \sqrt{s}, T)}{2},\end{aligned} \tag{14}$$

where $S_{q_1\bar{q}_1}$ and $S_{q_2\bar{q}_2}$ are the spins of $q_1\bar{q}_1$ and $q_2\bar{q}_2$, respectively. Even though the unpolarized cross section is calculated in the center-of-mass system, its frame independence and its dependence on the Mandelstam variable ensure that it can be used in any frame.

B. Numerical results

In Figs. 2-8 we plot unpolarized cross sections for the following nonresonant reactions: $\pi\pi \to \rho\rho$ for $I = 2$, $KK \to K^*K^*$ for $I = 1$, $KK^* \to K^*K^*$ for $I = 1$, $\pi K \to \rho K^*$ for $I = 3/2$, $\pi K^* \to \rho K^*$ for $I = 3/2$, $\rho K \to \rho K^*$ for $I = 3/2$, and $\pi K^* \to \rho K$ for $I = 3/2$. These reactions are endothermic, and the cross section for each reaction at a given temperature has at least one peak near the threshold energy $\sqrt{s_0}$. We use a function of the form $a\left(\frac{\sqrt{s}-\sqrt{s_0}}{b}\right)^c \exp\left[c\left(1-\frac{\sqrt{s}-\sqrt{s_0}}{b}\right)\right]$ to fit the numerical cross section. The parameters a, b, and c are adjusted to get the height, the width of the peak, and the peak's location on the $\sqrt{s}$-axis. The function with one peak can well fit some curves of which each has a peak, but is completely not enough to fit a curve with two peaks. To remedy this, we use a sum of two functions

$$\begin{aligned}\sigma^{\rm unpol}(\sqrt{s}, T) &= a_1\left(\frac{\sqrt{s}-\sqrt{s_0}}{b_1}\right)^{c_1}\exp\left[c_1\left(1-\frac{\sqrt{s}-\sqrt{s_0}}{b_1}\right)\right] \\ &+ a_2\left(\frac{\sqrt{s}-\sqrt{s_0}}{b_2}\right)^{c_2}\exp\left[c_2\left(1-\frac{\sqrt{s}-\sqrt{s_0}}{b_2}\right)\right],\end{aligned} \tag{15}$$

to get a satisfactory fit. This parametrization contains two terms. No more terms are used because of terrible computation time. Parameters' values are listed in Tables 1 and 2. We have calculated unpolarized cross sections only at the six temperatures $T/T_{\rm c} = 0$, 0.65, 0.75, 0.85, 0.9, 0.95. Unpolarized cross sections at any temperature that is between $0.65T_{\rm c}$ and $T_{\rm c}$ can be obtained via the linear interpolation or extrapolation among the cross

sections at the five temperatures $0.65T_{\rm c}$, $0.75T_{\rm c}$, $0.85T_{\rm c}$, $0.9T_{\rm c}$, and $0.95T_{\rm c}$. A procedure to achieve this can be found in Ref. [15]. The procedure needs the quantity d_0 what is difference of the peak's location on the $\sqrt{s}$-axis with respect to the threshold energy and the quantity $\sqrt{s_{\rm z}}$ what is the quare root of the Mandelstam variable at which the cross section is 1/100 of the peak cross section. The two quantities are listed in Tables 1 and 2.

C. Discussions

While $\sqrt{s}$ increases, $\int_0^\pi d\theta \mid \mathcal{M}_{\rm fi}(s,t) \mid^2 \sin\theta$ in the cross-section formula decreases slowly near the threshold energy and rapidly in the other region, and by contrast the factor $\frac{1}{s}\frac{|\vec{P}'|}{|\vec{P}|}$ increases very rapidly and decreases moderately. The peak of $\frac{1}{s}\frac{|\vec{P}'|}{|\vec{P}|}$ locates in the slowly-changing region of $\int_0^\pi d\theta \mid \mathcal{M}_{\rm fi}(s,t) \mid^2 \sin\theta$. Therefore, the peak of any curve in Figs. 2-8 near the threshold energy corresponds to the peak of $\frac{1}{s}\frac{|\vec{P}'|}{|\vec{P}|}$. In the present work we deal with meson-meson nonresonant reactions at low meson energies. Generally, only a small number of partial waves contribute to low-energy reactions [23]. Around the peak near the threshold energy, s waves of the scattering constituents (quarks and/or antiquarks) contribute to the cross section. While $\sqrt{s}$ is away from the threshold energy, p waves make a contribution to the cross section if a new peak is obvious, and d waves do if one more new peak is obvious.

Now we pay attention to changes of peak cross sections with respect to temperature in Figs. 2-8. The peak cross sections of $\pi\pi \to \rho\rho$ for $I = 2$, $KK \to K^*K^*$ for $I = 1$, $KK^* \to K^*K^*$ for $I = 1$, $\pi K \to \rho K^*$ for $I = 3/2$, and $\pi K^* \to \rho K^*$ for $I = 3/2$ have the same behavior: each decreases from $T/T_{\rm c} = 0$ to 0.85 and increases from $T/T_{\rm c} = 0.85$ to 0.95. While the temperature increases from zero, the long-distance part of the potential gradually becomes a distance-independent and temperature-dependent value, confinement becomes weaker and weaker, the Schrödinger equation produces increasing meson radii, and mesonic bound states become looser and looser. The weakening confinement with increasing temperature makes it more difficult to combine final quarks and antiquarks into mesons through quark rearrangement in $q_1\bar{q}_1 + q_2\bar{q}_2 \to q_1\bar{q}_2 + q_2\bar{q}_1$, and thus reduces cross sections. From $T/T_{\rm c} = 0$ to 0.85 the amount of peak cross section increased by the

slowly increasing radii of initial π and/or K mesons can not balance the amount reduced by the weakening confinement, and peak cross sections thus go down. From $T/T_{\rm c} = 0.85$ to 0.95 the amount of peak cross section increased by the rapidly increasing radii of initial π and/or K mesons overcomes the amount reduced by the weakening confinement, and peak cross sections thus go up. Similarly, we can understand that the peak cross section of $\rho K \to \rho K^*$ for $I = 3/2$ decreases from $T/T_{\rm c} = 0$ to 0.75 and increases from $T/T_{\rm c} = 0.75$ to 0.95 in Fig. 7.

In the above six reactions π and K appear only in the initial states. Unlike these reactions the reaction $\pi K^* \to \rho K$ for $I = 3/2$ has a pion in the initial state and a kaon in the final state. The slowly increasing K radius from $T = 0$ makes the kaon formation less affected by the weakening confinement. We thus get an increase in peak cross section from $T/T_{\rm c} = 0$ to 0.65. Depending on the amount of peak cross section increased by the increasing π radius and the amount reduced by the weakening confinement, there are a decrease in peak cross section from $T/T_{\rm c} = 0.65$ to 0.9 and an increase from $T/T_{\rm c} = 0.9$ to 0.95.

4. Summary

We have established the quark potential which is given by perturbative QCD with loop corrections at the short distance, becomes distance-independent and temperature-dependent at the long distance, and has the one-gluon-exchange spin-spin interaction smeared. The Schrödinger equation with the potential yields different temperature-dependent masses and different quark-antiquark relative-motion wave functions for different mesons. The potential, masses and wave functions in the transition amplitude developed from the quark-interchange mechanism give temperature-dependent unpolarized cross sections for the nonresonant reactions: $\pi\pi \to \rho\rho$ for $I = 2$, $KK \to K^*K^*$ for $I = 1$, $KK^* \to K^*K^*$ for $I = 1$, $\pi K \to \rho K^*$ for $I = 3/2$, $\pi K^* \to \rho K^*$ for $I = 3/2$, $\rho K \to \rho K^*$ for $I = 3/2$, and $\pi K^* \to \rho K$ for $I = 3/2$. The numerical cross sections are parametrized for convenient applications in hadronic matter in future. Every reaction takes a rise in peak cross sections while the temperature approaches the critical temperature.

ACKNOWLEDGEMENTS

This work was supported by the National Natural Science Foundation of China under Grant No. 11175111.

References

[1] Adler S S *et al.* (PHENIX Collaboration). Phys. Rev. C, 2004, 69: 034909

[2] Adams J *et al.* (STAR Collaboration). Phys. Rev. Lett., 2004, 92: 092301

[3] Fachini P (for the STAR Collaboration). Nucl. Phys. A, 2009, 830: 837c

[4] Aggarwal M M *et al.* (STAR Collaboration). Phys. Rev. C, 2011, 84: 034909

[5] Abelev B *et al.* (ALICE Collaboration). Phys. Rev. Lett., 2012, 109: 252301

[6] Barnes T, Swanson E S. Phys. Rev. D, 1992, 46: 131; Swanson E S. Ann. Phys. (N.Y.), 1992, 220: 73

[7] Barnes T, Swanson E S, Weinstein J. Phys. Rev. D, 1992, 46: 4868

[8] WONG C Y, Swanson E S, Barnes T. Phys. Rev. C, 2000, 62: 045201; Phys. Rev. C, 2001, 65: 014903

[9] Barnes T, Swanson E S, WONG C Y, XU X M. Phys. Rev. C, 2003, 68: 014903

[10] Li Y Q, XU X M. Nucl. Phys. A, 2007, 794: 210

[11] Karsch F, Laermann E, Peikert A. Nucl. Phys. B, 2001, 605: 579

[12] XU X M. Nucl. Phys. A, 2002, 697: 825

[13] Godfrey S, Isgur N. Phys. Rev. D, 1985, 32: 189

[14] WONG C Y. Phys. Rev. C, 2002, 65: 034902

[15] ZHOU J, XU X M. Phys. Rev. C, 2012, 85: 064904

[16] Buchmüller W, Tye S-H H. Phys. Rev. D, 1981, 24: 132

[17] Weinberg S. Phys. Rev. Lett., 1990, 65: 1177

[18] Brown G E, Lee C H, Rho M. Phys. Rev. C, 2006, 74: 024906

[19] QIU X J, XU X M. Nucl. Phys. A, 1990, 509: 769

[20] Mott N F, Massey H S W. The Theory of Atomic Collisions. Oxford: Clarendon Press, 1965

[21] Barnes T, Black N, Swanson E S. Phys. Rev. C, 2001, 63: 025204

[22] WONG C Y, Crater H W. Phys. Rev. C, 2001, 63: 044907

[23] Joachain C J. Quantum Collision Theory. Amsterdam: North-Holland Publishing Company, 1983

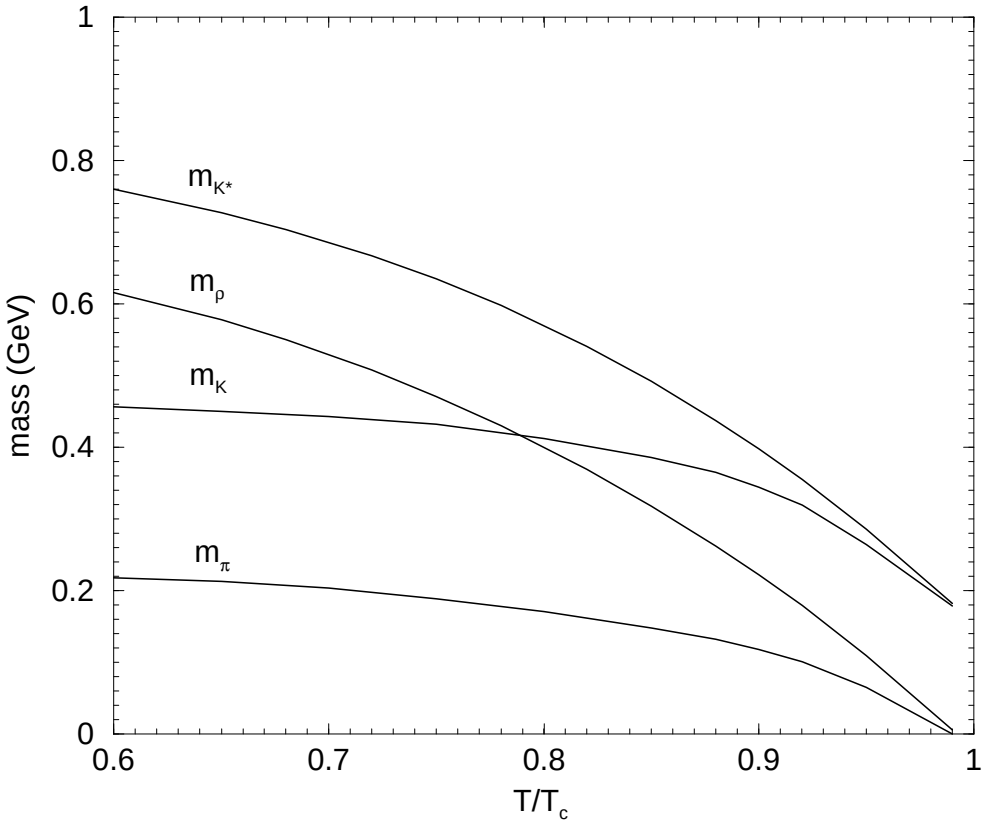

Figure 1: Meson masses as functions of $T/T_{\rm c}$.

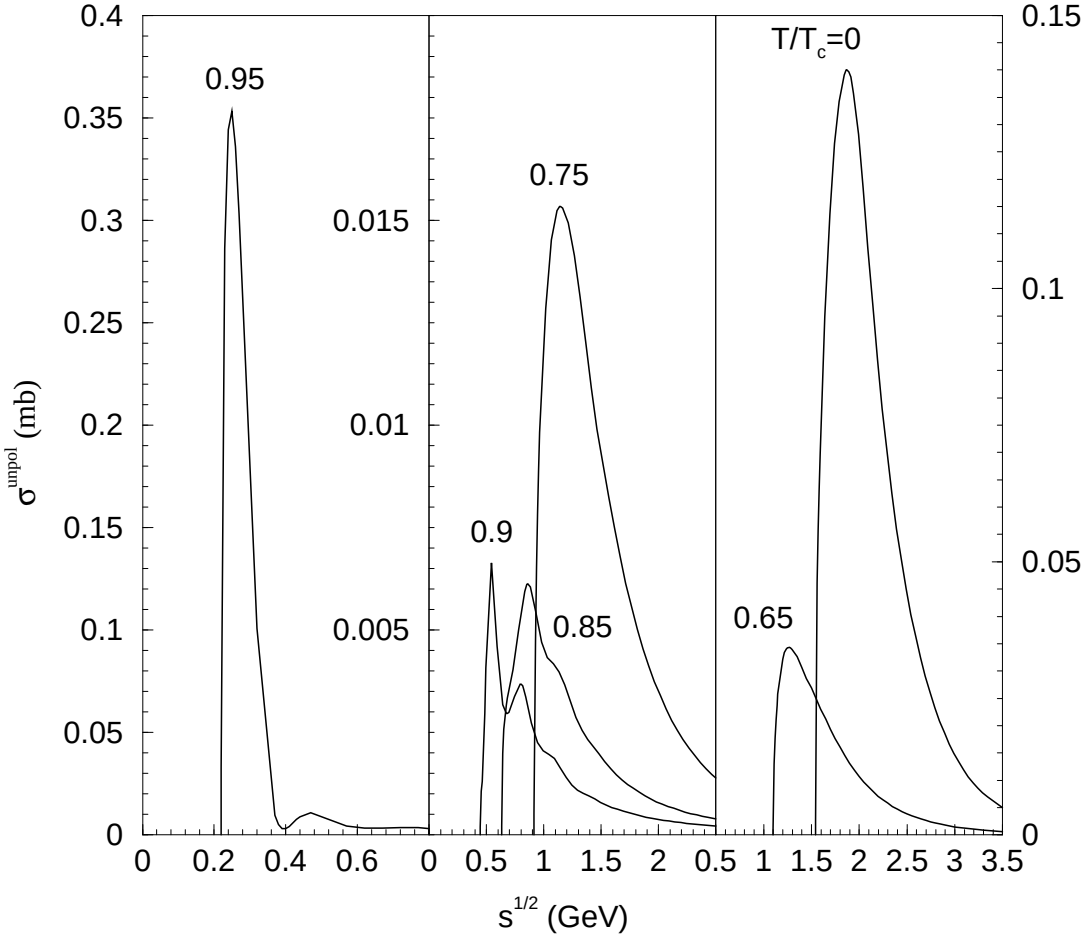

Figure 2: Cross sections for $\pi\pi \to \rho\rho$ for $I = 2$ at various temperatures.

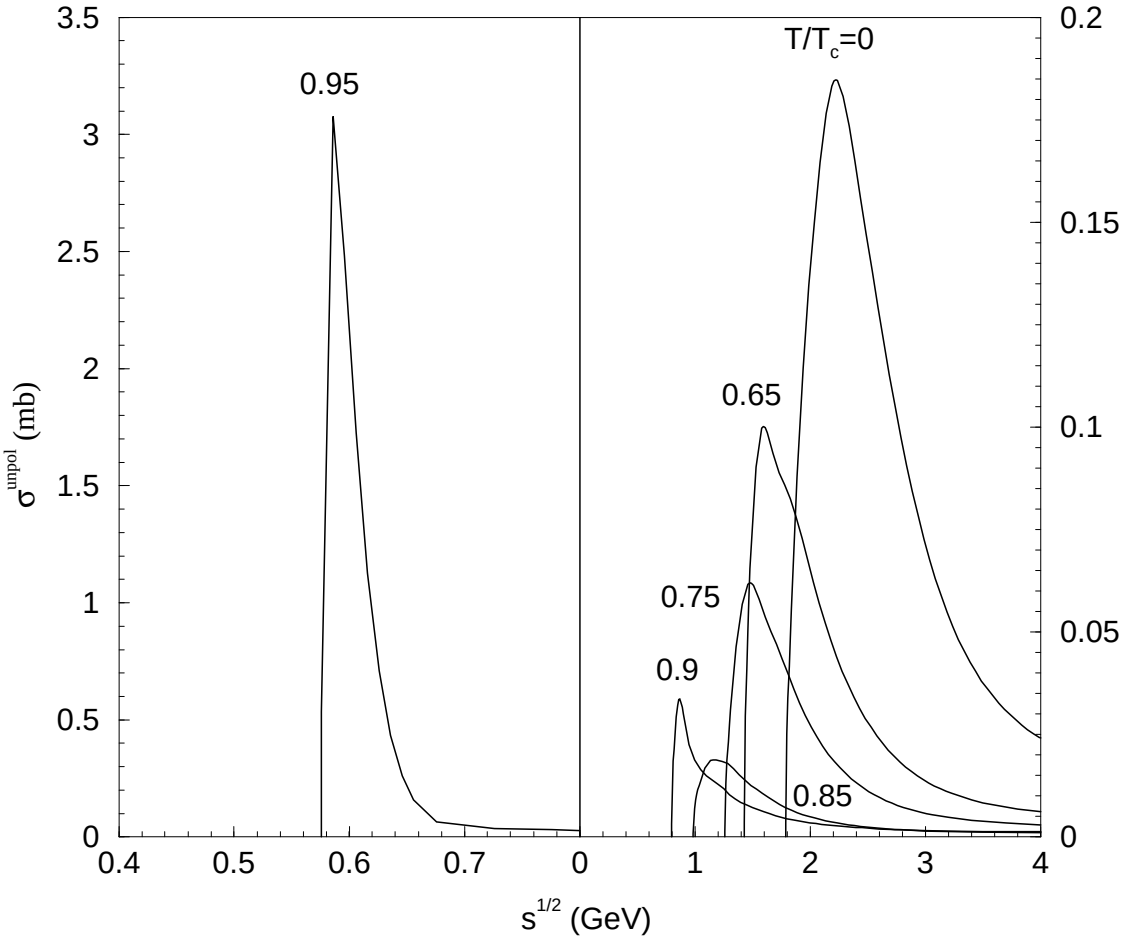

Figure 3: Cross sections for $KK \to K^*K^*$ for $I = 1$ at various temperatures.

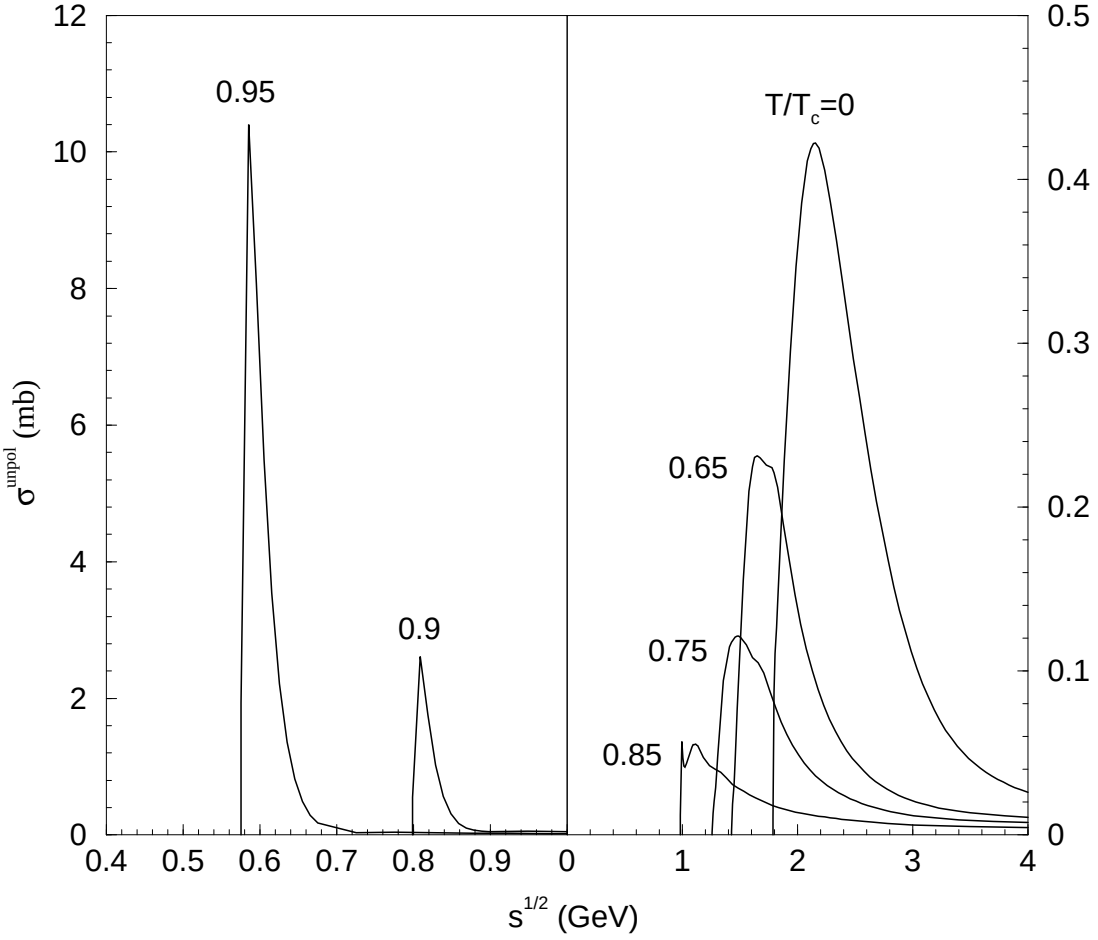

Figure 4: Cross sections for $KK^* \to K^*K^*$ for $I = 1$ at various temperatures.

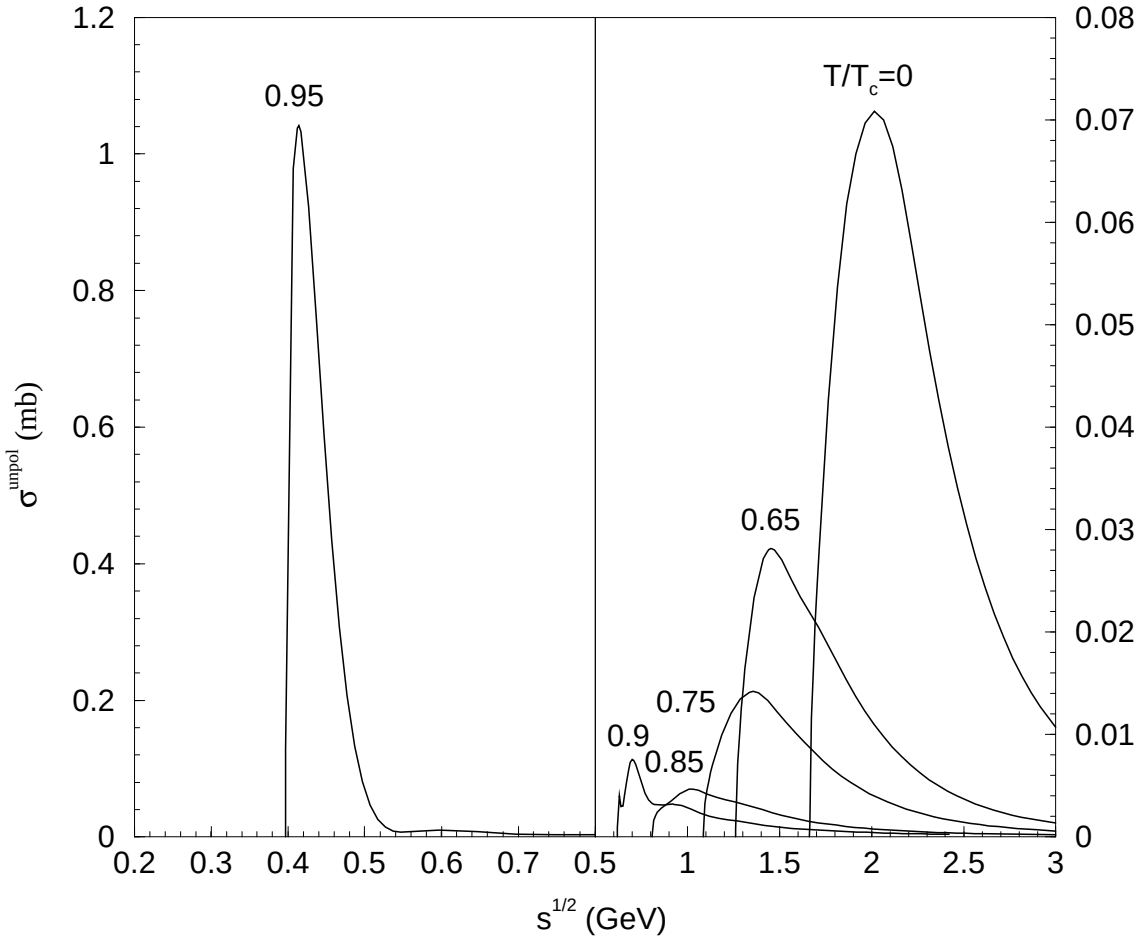

Figure 5: Cross sections for $\pi K \to \rho K^*$ for $I = 3/2$ at various temperatures.

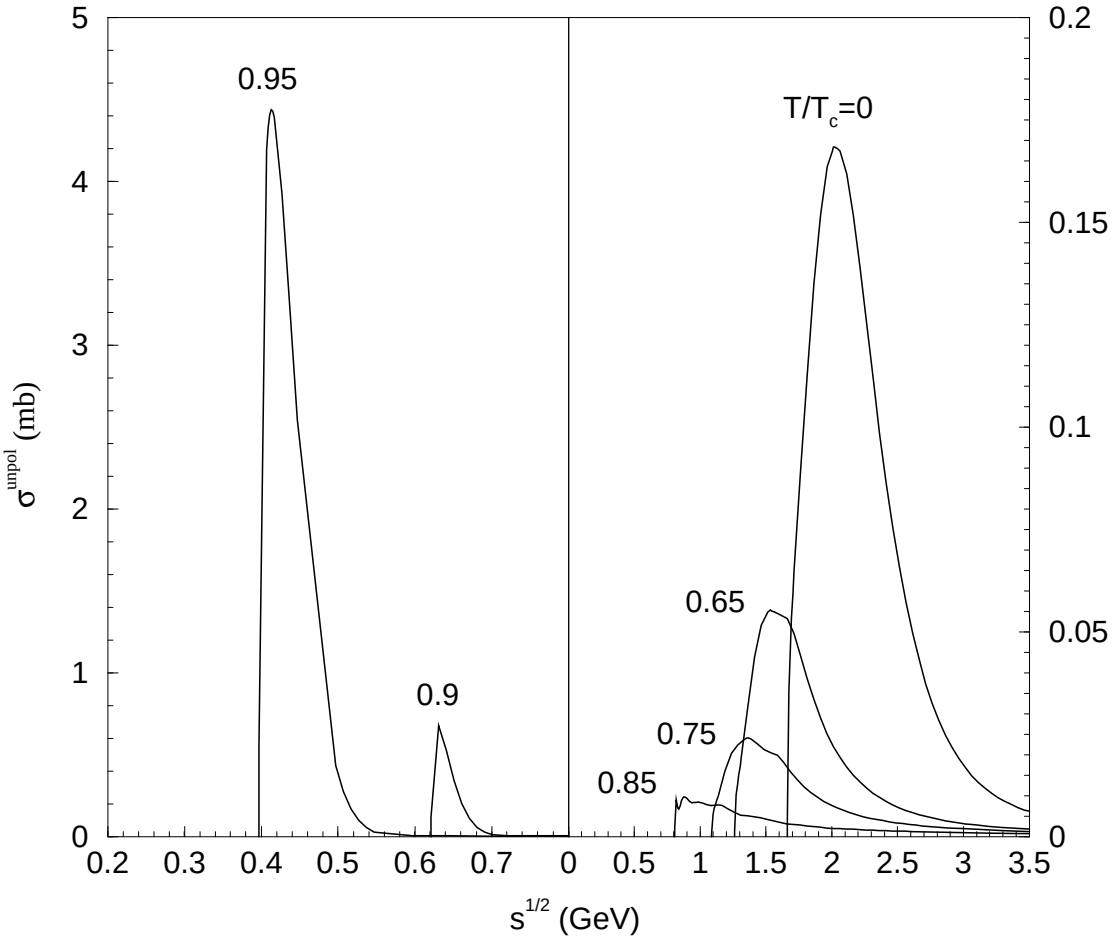

Figure 6: Cross sections for $\pi K^* \to \rho K^*$ for $I = 3/2$ at various temperatures.

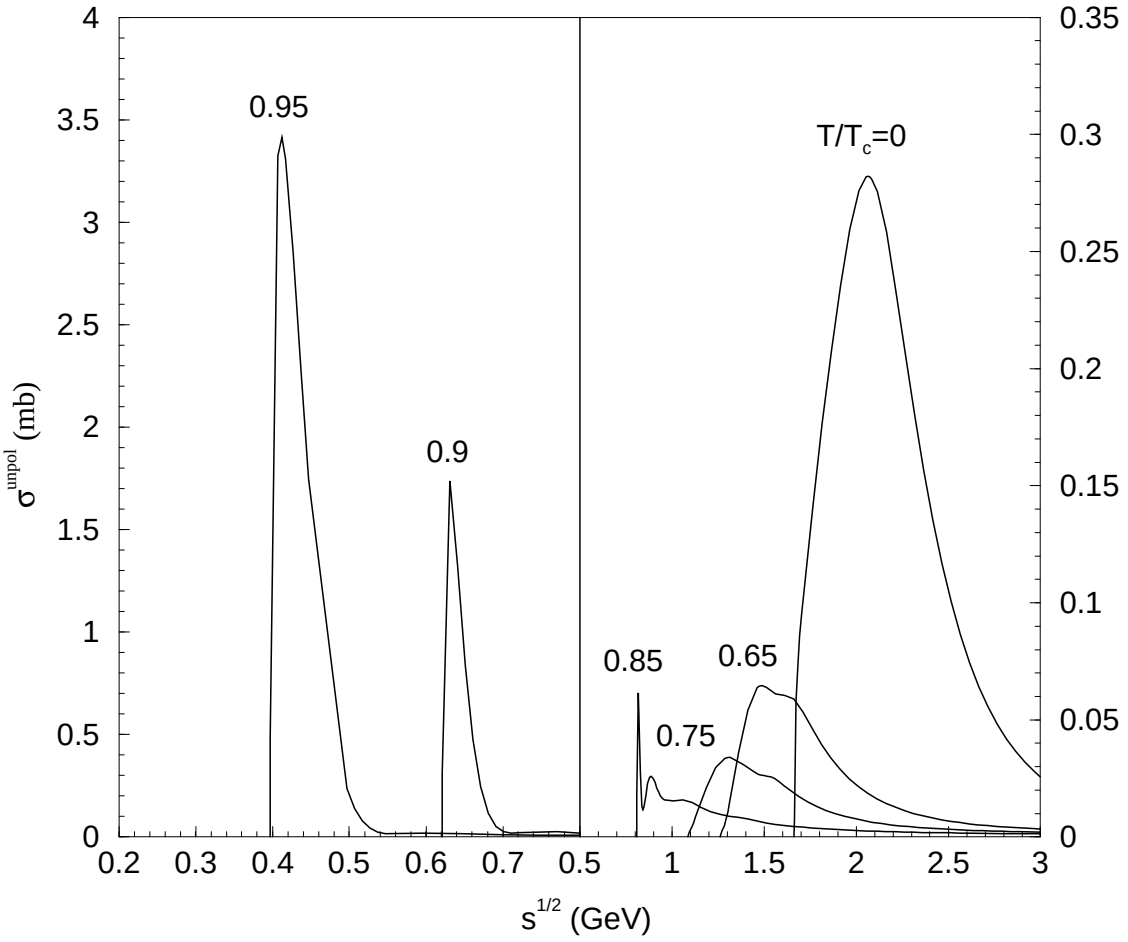

Figure 7: Cross sections for $\rho K \to \rho K^*$ for $I = 3/2$ at various temperatures.

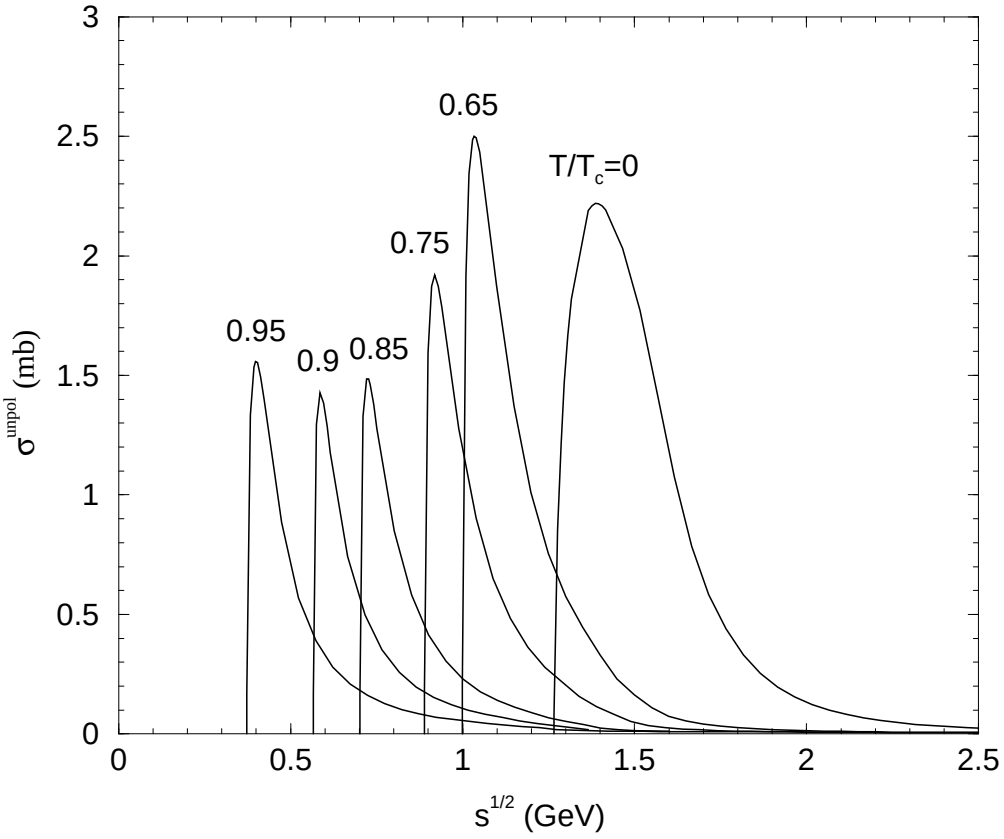

Figure 8: Cross sections for $\pi K^* \to \rho K$ for $I = 3/2$ at various temperatures.

Table 1: Values of the parameters in Eq. (15). a_1 and a_2 are in units of millibarns; b_1, b_2, d_0, and $\sqrt{s_z}$ are in units of GeV; c_1 and c_2 are dimensionless.

Reactions	T/T_c	a_1	b_1	c_1	a_2	b_2	c_2	d_0	$\sqrt{s_z}$
$\pi\pi \to \rho\rho$	0	0.09	0.17	0.56	0.06	0.44	1.91	0.33	4.272
	0.65	0.022	0.25	0.62	0.014	0.1	0.46	0.17	3.694
	0.75	0.01	0.19	0.45	0.005	0.24	0.91	0.22	3.221
	0.85	0.002	0.1	0.4	0.004	0.28	0.9	0.23	3.178
	0.9	0.0036	0.09	6.51	0.0032	0.33	0.42	0.1	3.113
	0.95	0.192	0.01	0.49	0.249	0.04	1.64	0.03	0.77
$KK \to K^*K^*$	0	0.12	0.44	1.43	0.06	0.32	0.41	0.44	5.21
	0.65	0.06	0.18	0.77	0.04	0.28	0.38	0.17	5.529
	0.75	0.03	0.23	1.3	0.03	0.25	0.45	0.22	5.73
	0.85	0.012	0.12	0.45	0.008	0.36	0.94	0.18	6.849
	0.9	0.018	0.057	0.88	0.014	0.14	0.26	0.07	8.208
	0.95	0.2	0.0003	3.8	3.1	0.009	0.52	0.01	0.777
$KK^* \to K^*K^*$	0	0.4	0.34	0.99	0.05	0.01	0.45	0.37	5.005
	0.65	0.19	0.25	1.69	0.05	0.44	0.44	0.22	5.997
	0.75	0.1	0.23	1.55	0.03	0.47	0.41	0.22	6.782
	0.85	0.039	0.008	0.3	0.047	0.18	0.9	0.13	7.671
	0.9	2.2	0.005	0.48	0.8	0.015	1.13	0.01	1.207
	0.95	8.4	0.009	0.59	2	0.007	0.26	0.01	0.701

Table 2: The same as Table 1.

Reactions	T/T_c	a_1	b_1	c_1	a_2	b_2	c_2	d_0	$\sqrt{s_z}$
$\pi K \to \rho K^*$	0	0.038	0.345	1.95	0.034	0.24	0.49	0.35	4.008
	0.65	0.018	0.2	0.47	0.01	0.21	1.5	0.19	3.836
	0.75	0.0091	0.21	0.5	0.005	0.288	2.27	0.27	3.878
	0.85	0.0009	0.28	3.5	0.00373	0.184	0.46	0.22	4.112
	0.9	0.0032	0.005	0.5	0.0061	0.081	2	0.08	3.031
	0.95	0.91	0.011	0.53	0.32	0.037	2.59	0.017	0.534
$\pi K^* \to \rho K^*$	0	0.16	0.38	2	0.05	0.05	0.49	0.36	4.032
	0.65	0.034	0.31	2.57	0.024	0.21	0.44	0.27	4.112
	0.75	0.0105	0.146	0.41	0.0159	0.38	2	0.28	4.352
	0.85	0.0038	0.0039	0.59	0.0092	0.134	0.32	0.07	4.819
	0.9	0.45	0.002	0.72	0.61	0.012	0.96	0.01	0.805
	0.95	0.3	0.001	0.006	4.2	0.017	0.68	0.016	0.542
$\rho K \to \rho K^*$	0	0.18	0.42	2.9	0.124	0.151	0.45	0.4	3.859
	0.65	0.0045	0.11	0.39	0.056	0.304	1.77	0.23	4.345
	0.75	0.0259	0.239	1.74	0.0084	0.802	0.44	0.23	4.858
	0.85	0.05	0.0029	0.31	0.022	0.097	1.41	0.08	5.728
	0.9	1.3	0.007	0.44	0.5	0.013	1.4	0.01	0.811
	0.95	2.2	0.002	1.32	3.4	0.015	0.58	0.015	0.532
$\pi K^* \to \rho K$	0	1.3	0.05	0.54	1.49	0.188	1.96	0.12	2.549
	0.65	0.97	0.1	0.66	1.8	0.027	0.49	0.035	1.812
	0.75	1.17	0.02	0.493	0.94	0.071	0.545	0.03	1.657
	0.85	0.9	0.018	0.53	0.7	0.056	0.44	0.02	1.494
	0.9	0.47	0.061	0.38	1.02	0.02	0.52	0.02	1.386
	0.95	1.02	0.022	0.55	0.6	0.054	0.39	0.025	1.314